PHYS3051 Lab Report 2
Antenna Radiation Patterns

Ryan White
s4499039
with partners Sascha Lawton, Ceri Harris

Semester 1, 2023

Abstract

Using different radius optical fibres, we analyse the mode-propagation of 633nm light via the projected radiation patterns on a screen. We find that single-mode optimised fibres yield an almost perfect Gaussian distribution in the output intensity pattern, while few and multi-mode optimised fibres are subject to significant constructive interference between the propagated modes which makes for a chaotic radiation pattern on the image screen. Using Gaussian fits to the data, we determine values for the numerical aperture and number of propagated modes to within σ of the respective accepted values for the single-mode fibre, but only within 2σ for the multi-mode fibre. Suggestions are made both to minimise noise in future analogous studies and also to derive more accurate values (for example, with the fibre acceptance angle) given the same signal-to-noise ratio in the data. Finally, we conclude that a single-mode optimised fibre is ideal for long range communications due to the power distribution and the linearly polarised nature of the signal due to the fibre geometry.

1 Introduction

Information transmission and communication forms much of the foundation on which the modern world is built. Having reasonably lossless point-to-point information transfer allows us to access high-speed internet or other forms of communication while remaining efficient in our energy cost to transmit data. Optical fibres are the answer to this information transmission, where light is guided through a translucent cable towards some destination. Transmitting light through an optical fibre allows speeds of significant fractions of c [4], while avoiding the loss of power associated with radiative transmission and the inverse square law. Understanding the specific physics of optical fibre transmission has implications for the efficiency of data transmission, as well as the nuances of interpreting the received data after transmission through the fibre. Herein we investigate the mode propagation through different waveguide configurations with red light in the optical spectrum, as well as the presence of a polarised output.

2 Theory

The basics of optical fibre light propagation are both reasonably simple and very well understood. At it's core, light from some medium is injected into a transparent fibre medium to which it travels along the cable axis with (ideally) total reflection against the fibres internal boundaries. Finally, the light will reach the end of the fibre and be able to be used for some application; in our case, we allow the light to re-enter its original medium (for which it was incident on the initial cable face) and observe its refraction effects and intensity profile.

As the light propagates through the fibre, its radial intensity profile within the fibre is dependent on the number of guided electromagnetic modes. Mostly used in telecommunications, optical fibres which only allow the fundamental mode to propagates are referred to as single-mode fibres [2]. For such single mode fibres, the power profile within the fibre and hence its projection is well approximated by a Gaussian function [4] of the form

$$f(x) = A \exp\left(-\frac{(x-\mu)^2}{2\sigma^2}\right) \tag{1}$$

where A is the peak intensity, and the other parameters correspond to their usual meanings. The standard deviation in this distribution (or in terms of a more physical meaning, its spread) is intrinsically linked to the width of the optical fibre core width. Intuitively, we would expect a smaller *absolute* spread in the power distribution for a thinner cable. Naturally you can't have a long-transmitting signal with a power-spread larger than the core width, but this is also due to the refraction and reflection effects that come with a smaller cable radius. Perhaps the most useful metric for how we numerically quantify how much light is accepted into the fibre (and hence will affect the power distribution) is given by the numerical aperture (NA) [2]:

$$\mathrm{NA} = n_{\mathrm{in}} \sin\theta_a \tag{2}$$

Here n_{in} is the refractive index of the medium in which the incident light on the fibre is propagating, and θ_a is the acceptance angle for incident light on the fibre face to be totally internally reflected at first reflection. As per the laboratory notes [4], we take the half-angular separation between the peak projection signal intensity and the 5% intensity to be the acceptance angle. Although this may seem unintuitive, due to the refraction of the incident light on contact with the fibre and the subsequent refraction of the propagated light out of the fibre back into the air (with the same refractive index as the initial incident light), the angular separation in the image between those two points is theoretically identical to that of the incident light acceptance angle. This method of determining NA may not apply in general, but is theoretically sound in the context of this experimental setup.

The number of modes that are 'allowed' to propagate within the fibre is dependent on the width of the fibre core and the wavelength of incident light. In practice, we use the so called V-number to estimate the number of modes that can propagate in a fibre [4], which, shown in equation (3), relies on the incident wavenumber (and hence wavelength) and the numerical aperture (and so also the fibre acceptance angle and core radius).

$$V = k_{\text{in}} a \text{NA}; \qquad M \simeq \frac{V^2}{2} \tag{3}$$

The projected radiation pattern for a high number of modes no longer adheres well to a Gaussian form as the signal is the superposition of all of the (polarised) modes onto the projection screen. In this large-mode limit, we approximate the number of modes in the fibre according to the M-number in equation (3) [4]. Generally the fundamental mode will still have the largest influence on the power distribution, but lower order modes add effectively random perturbations to the idealised Gaussian which influences prediction/fitting.

As the modes propagate the optical fibre, they are constantly being reflected internally off the fibre walls. Over many reflections, a polarisation in the propagated light is cultivated due to these boundary interactions [2]. As such, we'd expect a net linear polarisation for light transmitted through a sufficiently long fibre (even where the incident light has no net polarisation). With this in mind we'd expect the light passing through a linear polarisation filter to have an intensity (at the power distribution peak) according to Malus' law [1],

$$I = I_{\text{pol}} \cos^2(\theta - S) + I_{\text{unpol}} \tag{4}$$

where θ is the rotation of the filter, I_{unpol} is the base intensity of any unpolarised component of the light, I_{pol} is the intensity of the polarised component of the light, and S is the phase shift of the signal. It's most useful in our analysis to investigate the polarisation of single-mode fibres, as this fibre type is used for long-range communications [2] and hence subject to (in principle) the greatest induced polarisation in the transmitted signal.

3 Experiment

To analyse the light output through an the different optical fibres, we used a laser with output red light centered at (a quoted) 633nm and various optical fibres optimised for different wavelengths. Three fibre species were used: one which is capable of multi-mode propagation in the optical spectrum, one capable of few-mode propagation, and another for effectively single-mode transmission.

A cable mount was situated approximately inline with the laser output so that incident light could be coupled to and enter the cable waveguide. The orientation of the cable-end was able to be fine-tuned via bi-axial adjustments on the mount. That is, once the fibre was connected to the mount, turning fine dials allowed us to accurately couple the light into the fibre to achieve an image on the display screen. These dials angled the cable-end face in perpendicular directions to polar and azimuthal degrees of freedom in the coupling orientation.
Another mount was situated directly opposite an image screen so that the transmitted light could be displayed onto the screen and subsequently imaged for analysis. There was no real need to modify the orientation of the cable-end on this mount as the image display was not overly sensitive to the fine-adjustments of the mount dials. A standard external computer webcam was placed on the opposite side of the screen (relative to the fibre output) and pointed at the image screen. Having the translucent screen between the camera and fibre output allowed us to photograph the output without overly saturating the photograph pixels.

For the analysis of fibre output polarisation, we had access to a linear polarisation filter attached to a mount that we could firmly fix into the mounting plate. This filter was mounted between the fibre output and the photodiode, where the mean values on the photodetector screen provided the experimental data.

3.1 Method

Once the experimental apparatus was setup as in the body of the Experiment section, we began collecting data. To begin with, we coupled the multi-mode fibre with the incident laser output where the fibre end was mounted approximately 6cm from the image screen. Using the imaging software we then photographed

the output pattern on the image screen. The fibre end mount was then moved (along the line of sight with respect to the webcam and image screen) to a distance of approximately 10cm from the image screen, and the output once again photographed. This was repeated for the other distances of 14cm and 20cm to make a total of four images for the multi-mode output pattern.

Secondly, we uncoupled the multi-mode fibre cable from the two mounts and coupled the few-mode fibre available to us. We photographed the output pattern on the image screen (where the end mount was approx. 20cm from the image screen), and repeatedly altered the coil structure of the optical fibre to produce a different pattern, imaging the resultant pattern each time.

Following this, we removed the multi-mode fibre cable from the start and end mounts and then coupled the single-mode fibre to them. The situated the output mount 5.5cm from the image screen and photographed the output using the webcam. As in the multi-mode process, we moved the end-mount further away from the image screen to a distance of 16.5cm and imaged the output. This was repeated once more for a distance of 25.5cm.

In terms of the polarisation sub-experiment, a polariser was situated between the end-mount and a photodetector (instead of an imaging screen) so that we could alter the intensity of the output polarised light incident on the detector. Before we aligned the output and the detector, we noted the base induced voltage in the detector so that we could subtract this off of any obtained data. Finally, the output light and the detector were aligned (with the polarisation filter at the 0^o mark) and we noted the mean voltage in the photodetector display. We rotated the polariser in 30^o increments, and recorded the mean induced voltage each time until we had data for a full rotation of the polariser.

4 Results

All data analysis and plotting was contained within a Python script, where we utilised `matplotlib`, `numpy`, and `scipy` for the bulk of analysis. The optimally sliced row of the images was determined via a search algorithm which maximised the sum of the image red band pixels across the image horizontal axis. Given the quality of the data and the expected shape of the distribution, this should give the row with the highest peak as well as the largest angular extent for which the signal is spread across. An example of this is shown in Figure 1, and the sliced fibre output patterns are displayed in Figures 2 and 3.
On observation of the sliced data Gaussian fits, we can immediately note several key features about output radiation patterns. Firstly, we see that the output pattern due to the single-mode fibre is remarkably well approximated by a Gaussian, with χ^2_{dof} values reasonably close to the ideal 1 value. We justify the use of the χ^2 test statistic in our analysis due to the Normal data uncertainty, even in the red pixel values where uncertainties are inherently Poisson distributed (and hence approximately normal for values of $\gtrsim 10$). We've calculated the χ^2 values based on data points within 3σ of the mean (in terms of the data distribution), which we believe accurately corresponds to a high signal to noise subset of the entire data space. For values outside of this range, we argue that (in terms of the data) there is negligible presence of the output radiation pattern and is indicative only of the contaminant noise.
The acceptance angle for each data collection was determined based on the Gaussian fit to the data according to the method in the Theory section. On inspection of Figures 2 and 3, we can clearly see that the Gaussian fit aligns more closely to the data peak for the single-mode pattern. As alluded to in the Theory, this is due to the superposition of the signals in the multi-mode signal which deviates from an idealised Gaussian curve. Because of this, our estimated acceptance angle based on the fit has a larger value for the multi-mode curves than what we'd expect by looking at the raw data. Conversely, we see that the acceptance angle for the single-mode fits

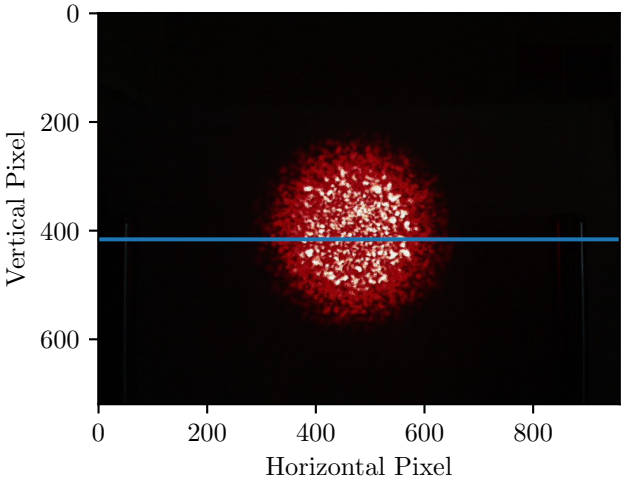

Figure. 1 The chosen horizontal slice of data used for each image in analysis was chosen via an algorithm that maximised the sum of the red band values in the pixels. This particular image corresponds to the multi-mode collection at a distance of approximately 14 ± 1.5cm. The images of each other multi-mode distance were analogous, just with different variances and peak values as in Figure 2. The same algorithm was used to characterise the single-mode images, although the output pattern more closely resembles a Gaussian as per Figure 3. Each collected image has a resolution of 960×720 pixels.

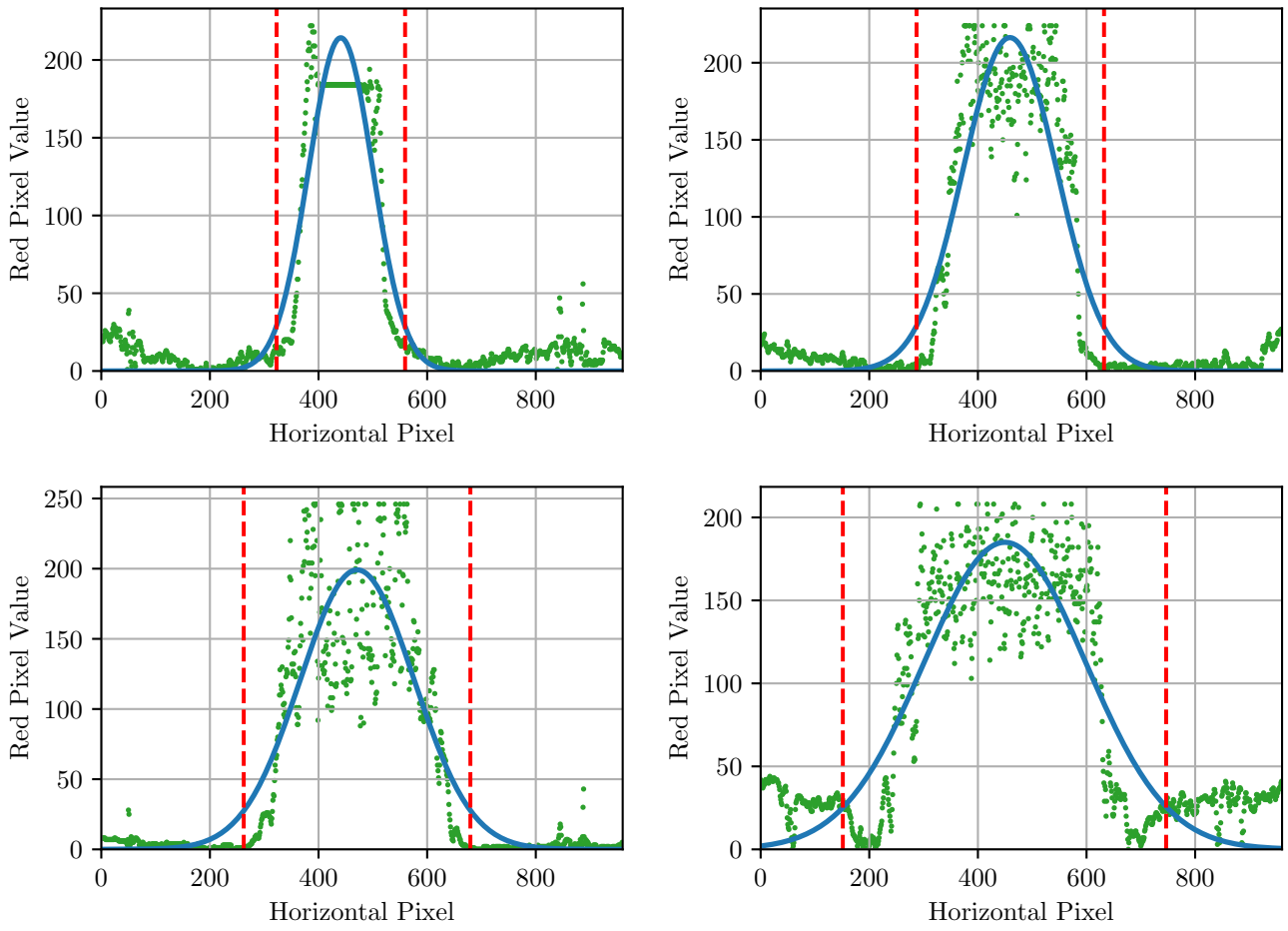

Figure. 2 Gaussian fits for the observed multi-mode output pattern, with calculated acceptance angles. From left to right, top down, the fits are for the observed beam where the fibre end was 6, 10, 14, and 20cm away respectively from the image screen (with uncertainties of ±1.5cm for each distance). The green points are the raw data, subject to Poisson uncertainty, the blue curve is the Gaussian fit onto the data, and the red dashed lines indicate the half-width angle (with respect to the mean) corresponding to the fibre acceptance angle. Mean fit parameters and their associated uncertainties were derived from a Monte Carlo pipeline on the data, and the yielded χ^2_{dof} results within 2σ of the mean for each respective fit are approximately 11.4, 15.7, 17.8, and 13.7.

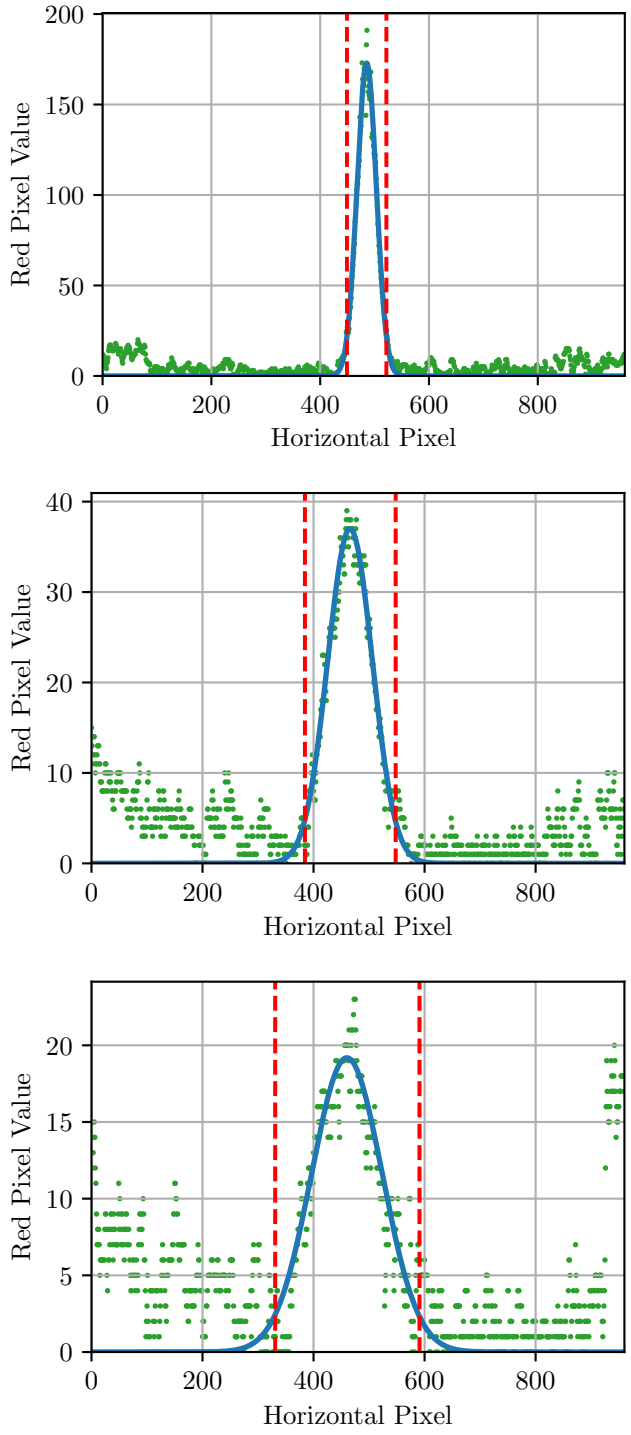

Figure. 3 Gaussian fits for the observed single-mode output patterns, with acceptance angles as described in Figure 2. In descending order, the data corresponds to fibre ends of 5.5, 16.5, and 25.5cm respectively (with uncertainties of ±1.5cm). The fits were obtained by the same Monte Carlo process mentioned earlier, with resulting χ^2_{dof} values (for within 2σ of the mean) of 0.43, 0.34, and 0.82 respectively.

aligns extremely well to what we'd expect for that data distribution.

Further adding to these inaccuracies in our multi-mode Gaussian fits, we note that a majority of pixels about the peak are saturated in our obtained images. This effectively truncated our y-data which naturally gave an inaccurate and much lower fit peak compared to the true peak.

Since the acceptance angle relies on both the peak value and the spread in the Gaussian fit, both of these issues gave us fairly inaccurate angles which propagated into the numerical aperture and subsequent calculations. Table 1 shows our calculated values for the relevant fibre parameters. The manufacturer specifies a value (without uncertainty) of NA = 0.012 for the single-mode fibre and NA = 0.290 for the multi-mode fibre [4]. Our found NA for the single-mode fibre is well within σ of the 'true' value, but just over 2σ out of agreement for the multi-mode fibre. As expected, the multi-mode fibre has large V and M numbers which is characteristic of a fibre with many mode propagation. We calculated a single-mode V-number which is interestingly greater than the $V_{\text{min}} \leq 2.405$ value quoted as being the minimum such that only the lowest order mode can propagate in the fibre [4]. For a fibre with width 4.3μm and NA = 0.12 as quoted by the manufacturer, we'd require a transmission wavelength of about 674nm to meet the minimum mode propagation threshold (compared to our 633nm light used in the experiment), although our value here is within σ of the quoted value.

Parameter	Single-Mode	Multi-Mode
Numerical Aperture	0.126 ± 0.020	0.359 ± 0.030
V-number	2.68 ± 0.40	179 ± 15
M-number	-	$(1.67 \pm 0.29) \times 10^4$

Table 1 Calculated numerical aperture (NA), V and M number values for each of the single and multi-mode fibres. The uncertainties in values were determined via a Monte Carlo algorithm using the Gaussian fit parameters derived from the data.

The polarisation data for the single-mode fibre is shown in Figure 4. We see an excellent fit of equation (4) – Malus' law – to our data across one rotation of the polarising filter. We clearly see that light transmitted via the single mode fibre is linearly polarised at an angle corresponding to the phase shift (as we'd expect a non-shifted wave to begin at the maximum value), although not entirely polarised. The degree of polarisation is calculated with an extinction ratio of $r_e = 7.7 \pm 1.1$. That is, the maximum intensity (when the polarisation filter aligns with the angle of light polarisation) is almost 8 times that of the base intensity (that of the unpolarised component in the light. In our analysis here, we subtracted the ambient baseline voltage in the photodetector out

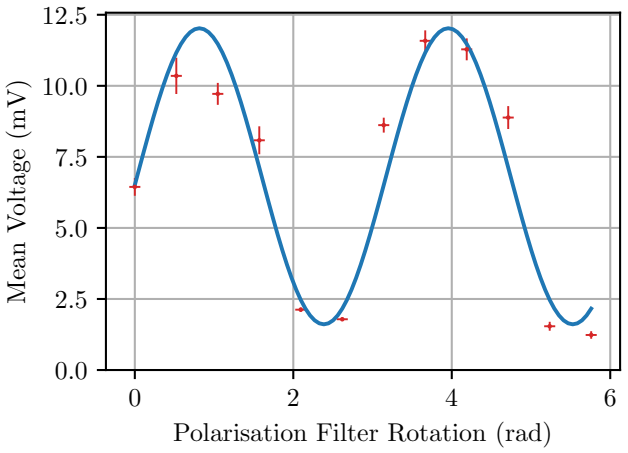

Figure. 4 The induced current in the photodiode detector due to the output light through a polarisation filter was fit against a squared cosine function. Uncertainties in the data were estimated via statistics on like-data points in the data collection, where the sinusoidal fit (and the error in its parameters) were obtained via a Monte Carlo pipeline. We note a peak height of 10.4 ± 0.4mV, a phase shift of 0.81 ± 0.03 radians, and a base voltage of 1.58 ± 0.26mV for the best-fit parameters. The fit according to Malus's Law, or equation (4), is characterised by $\chi^2_{\text{dof}} \simeq 0.21$ due to the model overfitting the few and sparse data points.

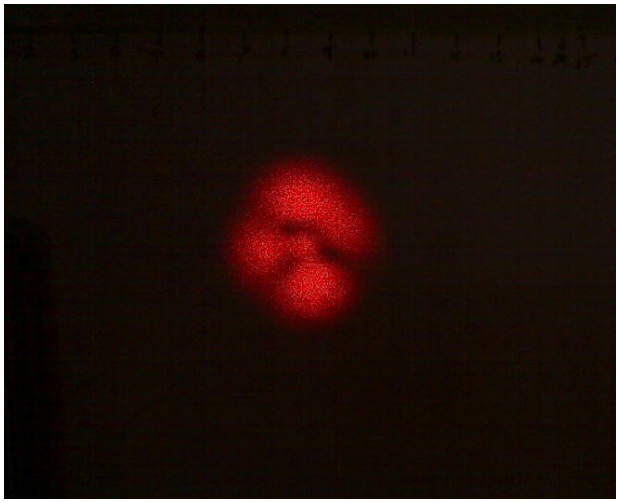

Figure. 5 The output patterns from the few-mode fibre depend on the coil structure through which the light propagates. Here we see a pattern likely corresponding to a 4-mode pattern, more specifically LP_{42} or LP_{23}. An animation of the variation in output pattern with changing coil structure is shown in this link. The animation shows varying low-order LP modes, including a clear third order mode likely corresponding to LP_{31} and/or LP_{32} [3].

from our data, which had a value of $V = 3.15 \pm 0.15$mV (where the uncertainty was based on the time-series variance in recorded values over a period of minutes).
An example of a few-mode projection pattern is shown in Figure 5. As the caption suggests, we see modes in our data corresponding to a V-number of at *least* $V \sim 10$. This fits within expectations of a V-number for the few-mode fibre between that of the single and multi-mode fibres. As the animation shows, the projected pattern was very sensitive to changes in the coil structure; as the geometry of the entire cable coil was altered, constructive (and by extension destructive) interference occurs throughout the light transmission due to the changing number of reflections in each mode, which significantly influences the final image as the light exits the fibre.

5 Discussion

Our image on the screen was subject to slight diffuse contamination due to the output from the laser itself, as no opaque surface was placed between the screen and laser. In future experiments, this is a key recommendation to improve the signal to noise ratio of the obtained data. Further, we note that the multi-mode fibre output was particularly saturated due to the more numerous mode propagation and consequent light intensity on the image screen. Since the imaging software (via the Windows operating system and webcam GUI) did not allow us to change the image exposure due to a bug, this experimental shortfall was unavoidable. We recommend imaging with a more sophisticated setup in future experiments, perhaps with a CCD where the exposure is more customizable, and the theory relating to the physics of each pixel is well understood.

We suggest for future experiments using the same setup/equipment to implement a different method of inferring the acceptance angle in the multi-mode data. Our best suggestion is to create a linear search algorithm which iterates over an ordered data set to find the first maximum value in some spatially-moving-averaged data, and then iterating backwards to find where the 0.05% value occurs. We note that this functionality is already somewhat implemented with the `numpy.where()` function, which returns an ordered array of values corresponding to a desired value (in our case, we would want the first maximum of the data). To further validate the returned value in this case, we note that the data distribution is (to a good approximation) symmetric and so the algorithm could be applied to the forward and backward iterations over the entire dataset. Finally, we note that the truncated distribution that we see in our multi-mode data could instead be fit to two exponential functions for the data curve up the would-be Gaussian. Since Gaussian functions are fundamentally described by exponentials, we expect this could give a much more

reasonable estimate for the acceptance angle in future studies. We expect that a Monte Carlo analysis would be ideal in terms of time and accuracy in estimating the uncertainties in all of these suggested methods.

6 Conclusions

We analysed the projected radiation pattern of a 633nm wavelength laser through single, few, and multi-mode optical fibres, and conclude that a single-mode fibre (for a given wavelength of light) is ideal for long range, predictable information transmission. Since only a single mode is reliably propagated through this width of fibre, the resultant power distribution at the end of the fibre is effectively unaffected by constructive interference from other propagated modes, giving an idealised Gaussian radiation pattern to an excellent approximation. On top of this, we find that the single-mode fibre output is linearly polarised at almost $\pi/4$ radians for our specific fibre, with an extinction ratio of almost 8 indicating that signals sent in communications (over much larger length fibres than our setup) are significantly polarised.

Finally, we found that few and multi-mode projections were incredibly sensitive to the fibre coil-structure through which the light propagated. Even a small perturbation in the tightness of the coils would significantly affect the dominant mode for the few-mode fibre, and would give a different 'noise' distribution in the multi-mode projection. While our few-mode analysis was effectively qualitative, our multi-mode analysis was significantly impacted by noise in the data. We suggest data-analysis techniques in future analogous studies which may yield better results with like-data.

References

[1] Edward Collett. *Field Guide to Polarization*. SPIE, Sept. 2005. DOI: 10.1117/3.626141. URL: https://doi.org/10.1117/3.626141.

[2] Gerd Keiser. *Fiber Optic Communications*. Springer Singapore, 2021. DOI: 10.1007/978-981-33-4665-9. URL: https://doi.org/10.1007/978-981-33-4665-9.

[3] Rudiger Paschotta. *Fibers*. Apr. 2023. URL: https://www.rp-photonics.com/fibers.html.

[4] PHYS3051. *Fields in Physics Laboratory – Optical Fibre Modes*. 2015.